Simulation of the turbulent flow over an array of flexible blades

Silvio Tschisgale

Institute of Fluid Mechanics
Technische Universität Dresden
George-Bähr-Str. 3c, 01069 Dresden, Germany
silvio.tschisgale@tu-dresden.de

Richard Meller

Institute of Fluid Dynamics
Helmholtz-Zentrum Dresden-Rossendorf
Bautzner Landstr. 400, 01328 Dresden, Germany
r.meller@hzdr.de

Jochen Fröhlich

Institute of Fluid Mechanics
Technische Universität Dresden
George-Bähr-Str. 3c, 01069 Dresden, Germany
jochen.froehlich@tu-dresden.de

INTRODUCTION

Aquatic ecosystems constitute a key topic due to their abundance and their various roles on different scales, ranging from the quality of drinking water taken from the local river to the large-scale impact on climate change. The fluid mechanical interaction between the flow and the flexible plants in an aquatic canopy is a key element determining hydraulics, as well as the transport of sediment, nutrients, and pollutants. In order to fully understand the mutual interaction between the fluid flow and the plants a detailed analysis of the generated three-dimensional flow data is of crucial importance.

This work presents a numerical method which is well suited for simulations of abstracted aquatic canopy flows in the framework of a Large Eddy Simulation. It is employed to simulate the turbulent flow over a model canopy of 800 flexible blades at a Cauchy number of 16.5 which is the largest canopy-resolving simulation of this type done so far. The simulation data are analysed to get a deeper understanding of the physics of aquatic canopies, e.g., concerning the existence and shape of coherent vortex structures.

PHYSICAL AND NUMERICAL MODEL

The physical problem addressed consists of a Newtonian viscous fluid of constant density interacting with an array of elastic blades. The governing equations for the fluid motion are the unsteady three-dimensional Navier-Stokes equations

$$\frac{\partial \mathbf{u}}{\partial t} = -\nabla\cdot(\mathbf{uu}) + \frac{1}{\rho_f}\nabla\cdot\tau + \mathbf{f} \quad , \tag{1}$$

$$\nabla\cdot\mathbf{u} = 0 \tag{2}$$

where $\mathbf{u} = (u,v,w)^T$ is the velocity vector in Cartesian components along the Cartesian coordinates x,y,z, while t represents the time, p the pressure, ρ_f the fluid density, τ the hydrodynamic stress tensor, and $\mathbf{f}$ a mass-specific force. These equations are solved with the in-house code PRIME which is based on a second-order finite volume approach on a staggered Cartesian Eulerian grid with constant step size Δx in all directions for the spatial discretization and a semi-implicit second-order scheme for the time integration (Kempe & Fröhlich, 2012). In cases where a Direct Numerical Simulation (DNS) is not feasible, the Large Eddy Simulation (LES) approach is employed with the Smagorinsky subgrid scale model and a global Smagorinsky constant, C_s, tailored to the specific physical problem. The blades considered are geometrically characterized by their length which is far longer than their width and their thickness, hence a particular kind of rods. For the modeling of such rods a certain number of approximations allows replacing the fully three-dimensional representation of the body by a one-dimensional rod model. Several models of this type exist. The one applied here is the geometrically exact Cosserat rod model, which is suitable for rods undergoing large deflections (Simo, 1985; Antman *et al.*, 2005). The corresponding differential equations of motion are

$$\rho_s A\,\frac{\partial^2 \mathbf{c}}{\partial t^2} = \frac{\partial \hat{\mathbf{f}}}{\partial s} + \tilde{\mathbf{f}} \tag{3}$$

$$\rho_s\left(\mathbf{i}\,\frac{\partial \omega}{\partial t} + \omega\times\mathbf{i}\omega\right) = \frac{\partial \hat{\mathbf{m}}}{\partial s} + \frac{\partial \mathbf{c}}{\partial s}\times\hat{\mathbf{f}} + \tilde{\mathbf{m}}\,, \tag{4}$$

where $\mathbf{c}$ is the position of the center line, with the arc length s. The motion of the center line is governed by (3) and depends on the internal forces $\hat{\mathbf{f}}$ and the external forces $\tilde{\mathbf{f}}$. The cross section of the rod is assumed to be rigid and plane throughout the deformation. The local angular velocity ω depends on the internal forces $\hat{\mathbf{f}}$ and the internal moments $\hat{\mathbf{m}}$, as well as the external moments $\tilde{\mathbf{m}}$, as described by (4), with $\mathbf{i}$ the tensor of inertia in the global frame. The rods considered here have constant geometrical properties, i.e. constant cross sectional areas A, constant material properties such as the density ρ_s, and a linear viscoelastic material behavior of Kelvin-Voigt type over their entire length. With these assumptions, the equations of motion (3), (4) are solved numerically by an algorithm according to Lang *et al.* (2011). It is based on a finite-difference method and a special description of the rotations of the cross sections by quaternions.

The physical coupling of the continuous fluid phase and the rods is accomplished by the no-slip condition $\mathbf{u}(\mathbf{x},t) = \mathbf{u}_\Gamma(\mathbf{x},\mathrm{t})$, where $\mathbf{u}_\Gamma$ denotes the velocity of a point $\mathbf{x}$ on the surface of the rod. Numerically, the coupling is realized by an immersed boundary method (IBM), where the force $\mathbf{f}$ in the momentum balance of the fluid (1) is appropriately adjusted in each time step to enforce the no-slip condition at the immersed boundary. In this work it is assumed, that the grid spacing Δx is fine enough to reproduce the near-wall flow along the blades. As is well known, the standard Smagorin-

sky model causes non-physical values of the eddy viscosity ν_{sgs} in the near-wall region of any embedded immersed boundary. For this reason, a damping function is introduced here which smoothly switches off ν_{sgs} in the range of a few steps of the Eulerian grid on both sides of the blades, similar to a Van Driest damping function.
Besides the mutual interaction between the fluid and the structures, the latter are able to interact with each other due to collisions. This is taken into account by an appropriate collision model based on the work of Guendelman *et al.* (2003). The equations to be solved for multiple collisions result in an optimization problem (Tonge *et al.*, 2012) numerically treated by an iterative projected Gauß-Seidel method.
The solver was validated with various FSI test cases, such as the two-dimensional benchmark of Turek & Hron (2006). To demonstrate the suitability of the proposed method for flexible blades in cross flows considered in this work, an LES of the experimental setup of Luhar & Nepf (2011) with a single flexible blade in cross flow was performed (Fig. 1). The numerical results obtained are in very good agreement with the experimental data over a wide range of bulk velocities and Reynolds numbers. Already for moderate grid resolutions of about $W/\Delta x = 10$ grid cells over the blade width W the physical behavior of the blades is captured fairly well. This allows simulating large-scale FSI problems with large numbers of blades demonstrating that the method is well suited for canopy flows.

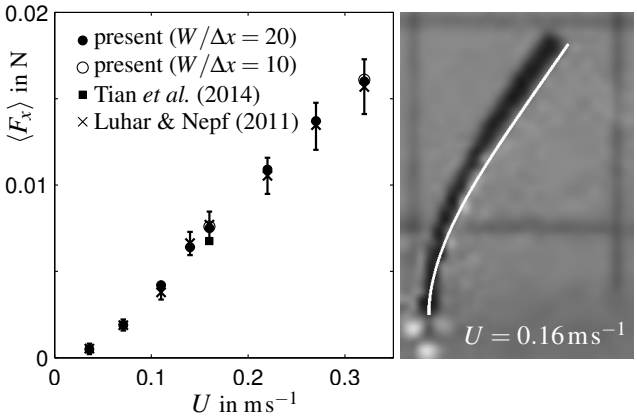

Figure 1. Flexible blade in cross flow, corresponding to the experimental setup of Luhar & Nepf (2011). Left: Time averaged drag force in streamwise direction, $\langle F_x \rangle$, for selected fluid bulk velocities U. The simulation results obtained for two grid resolutions are compared to the experimental data of Luhar & Nepf (2011) and to the simulation of Tian *et al.* (2014) for $U = 0.16\,\mathrm{m\,s^{-1}}$ (error bars from the experiment). Right: Comparison of the blade deflection between the experiment (black line) and the simulation (white line) for a velocity of $U = 0.16\,\mathrm{m\,s^{-1}}$.

RESULTS FOR AQUATIC CANOPY FLOW

The aim of this work is to develop a deeper understanding of the physics of flow-biota interaction in submerged canopy flows. Especially for such configurations the proposed numerical method is designed for: The interaction of numerous highly flexible slender structures in turbulent flow. To validate the solver a setup of the experimental work of Okamoto & Nezu (2010*a*) was simulated. This case was chosen as it exhibits the so-called *monami* phenomena (mo=aquatic plant, nami=wave), i.e. a strong relation of coherent vortices and an organized wavelike plant deflection (Okubo & Levin, 2001). Similar but mechanically different is the so-called *honami* phenomena observed in terrestrial canopies, e.g. cereals.

A sketch of the numerical setup simulated is given in Fig. 2. All relevant geometrical and material properties of the blades and the fluid are listed in Table 1. The dimension of the computational domain is $6H \times H \times 3H$ in x-, y-, z-direction. It was discretized by cubic cells of size $\Delta x = 0.625\,\mathrm{mm}$, i.e. $W/\Delta x = 12.8$ grid cells over the blade width. This yield 700 million grid cells which is at the very edge of what is technically feasible because the instantaneous flow has to be simulated over a certain duration to be developed and to accumulate statistics. Indeed, just a further halving of the grid spacing would yield 5.6 billion grid cells. To model the subgrid scale a Smagorinsky constant of $C_s = 0.15$ was chosen, as already employed by Okamoto & Nezu (2010*b*) for an LES of canopy flows over rigid blades. The 800 equally distributed strip-shaped flexible blades are discretized by 30 elements each in longitudinal direction. For the temporal discretization the time step was automatically adjusted to yield a CFL number of 0.5. The flow is driven by a spatially constant volume force - similar to a gravitational force - which is dynamically adjusted in time to maintain a constant bulk velocity of U. While a no-slip condition is applied at the bottom wall the water surface is approximated by a free-slip rigid lid condition. All remaining boundaries are periodic. The Reynolds number, based on the channel height, is $Re_H = UH/\nu = 42000$ and the Cauchy number $Ca = 6\rho_f U^2 L^3/ET^3 \approx 17$.

Table 1. Physical quantities according the experimental setup of Okamoto & Nezu (2010*a*) for a canopy consisting of flexible rectangular blades made out of polyester overhead projector (OHP) slides.

physical quantity	value	description
L	70 mm	blade length
W	8 mm	blade width
T	0.1 mm	blade thickness
ΔS	32 mm	blade spacing
H	210 mm	channel height
ρ_f	$1000\,\mathrm{kg\,m^{-3}}$	fluid density
ν	$1 \times 10^{-6}\,\mathrm{m^2\,s^{-1}}$	fluid viscosity
U	$0.2\,\mathrm{m\,s^{-1}}$	bulk velocity
ρ_s	$1400\,\mathrm{kg\,m^{-3}}$	blade density
E	4.8 GPa	Young's modulus
g	$9.81\,\mathrm{m\,s^{-2}}$	gravity

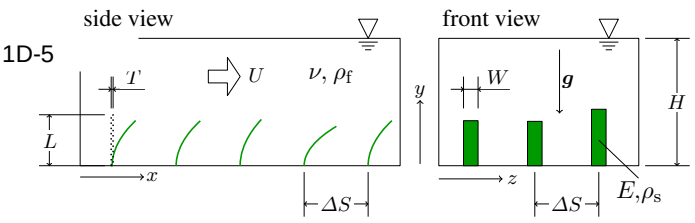

Figure 2. Numerical setup of the aquatic canopy modeled as an array of flexible blades with fixation on the bottom plate in squares (same ΔS in x and z), corresponding to the experimental setup of Okamoto & Nezu (2010*a*) with an overview over the physical parameters.

The simulation results for the time-averaged velocity profile and all relevant Reynolds stresses are given in Fig. 3. Moreover, the normalized profile $\langle u\rangle/U$ and the turbulent shear stress $\langle u'v'\rangle/U^2$ are compared to the experimental data. The comparison shows that the mean velocity component $\langle u\rangle$ is slightly underestimated inside the canopy region, while, consequently, it is slightly overestimated above the canopy in the free flow region. In terms of the Reynolds stress $\langle u'v'\rangle$ the maximum value is nearly equivalent to the experimental observation. Near the bottom wall the measurements behave differently up to a height of about $0.5L$. In the free flow region above the canopy $\langle u'v'\rangle$ behaves linearly, as required by the momentum balance. The experimental data, however, match this behavior only with some deviation. Hence, it must be assumed that the experimental statistics are not fully converged. For the remaining Reynolds stresses no experimental data are available.

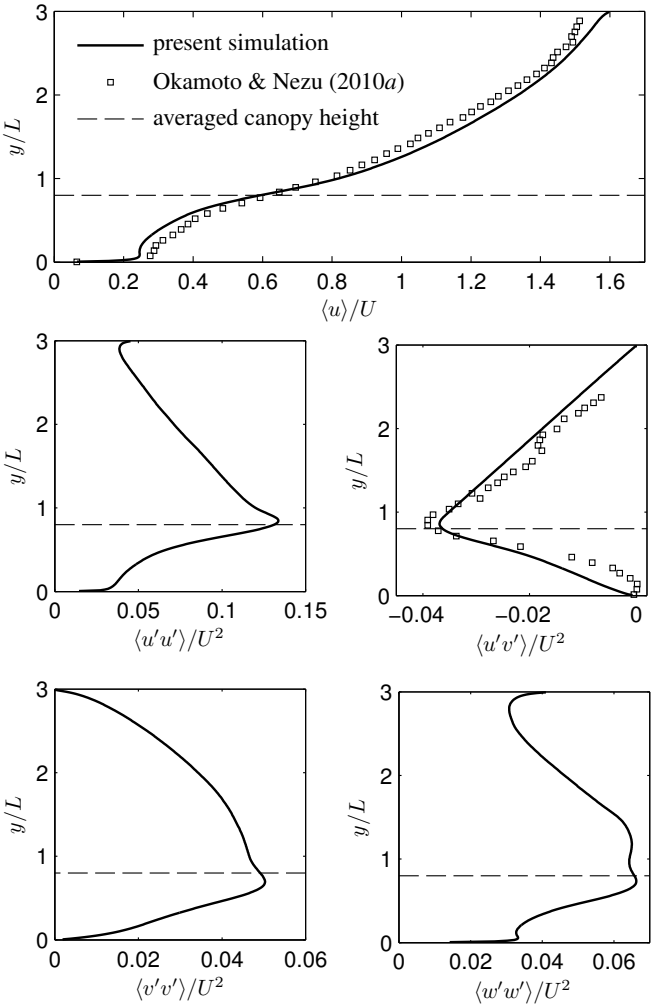

Figure 3. Normalized averaged velocity profile $\langle u\rangle/U$ and non-vanishing Reynolds stresses $\langle u'u'\rangle$, $\langle u'v'\rangle$, $\langle v'v'\rangle$ and $\langle w'w'\rangle$ normalized by U^2 (observe the different range). The present results are compared to the experimental data of Okamoto & Nezu (2010*a*) identified by black squares. The temporally and spatially averaged height of the canopy with the blades being deflected by the flow $\langle h_c\rangle/L = 0.8$, is represented by the dashed line. The value is exactly the same as in the experiment.

All results presented were obtained with the finest technically feasible grid resolution. To examine their sensitivity with respect to the grid employed, simulations with coarser resolutions were performed, presented in Fig. 4 (left). Even if the simulation results are still not fully converged in terms of the spatial resolution, the variations are comparably small. In addition, the influence of the Smagorinsky constant C_s was studied. As demonstrated in Fig. 4 (right), a change in C_s does not affect the velocity profile.

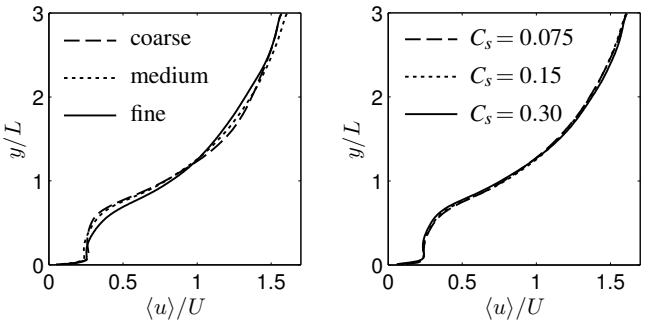

Figure 4. Influence of grid resolution (left) and value for the Smagorinsky constant C_s (right) on the averaged velocity profile $\langle u\rangle/U$. The tests were performed with a smaller computational fluid domain of size $3H \times H \times 1.5H$, i.e. half the size in the horizontal directions. The finest grid spacing Δx is defined by $W/\Delta x = 12.8$ grid cells over the blade width W, while for the medium and coarse grid the spacing was doubled once and twice, respectively. The variation in C_s was performed for the medium grid resolution.

Coherent structures

As demonstrated by Okamoto & Nezu (2010*b*) the monami phenomenon can be observed for the present set of parameters. It is characterized by a wavy deflection of a group of blades due to certain coherent velocity structures. The present simulation shows these well-separated regions of different blade deflection very nicely as they travel through the canopy (Fig. 6, left). A deeper analysis of the data reveals that these regions are accompanied by separated longer streaks of positive and negative velocity fluctuations $u' = u - \langle u\rangle$ (Fig. 6, right). For negative fluctuations $u' < 0$ the resulting decreased drag yields more erect blades, while for $u' > 0$, in turn, the blades are more deflected. These regions are usually termed low-speed (L-S) velocity streaks and high-speed (H-S) velocity streaks, respectively. As shown in Fig. 6 often H-S streak borders on a L-S streak and *vice versa*. It seems, that large-scale vortices primarily develop at these borders due to increased shear. Whether and how such vortices are correlated to a maximum deflection of the blades and the *monami* event remains to be investigated.

Already in 2009, Finnigan *et al.* elucidated the formation of vortices for terrestrial canopies. In that work, they deduced the eddy structures by means of conditional averaging of the flow field, using canopy pressure maxima as a trigger to identify the structure location. Based on the averaged results, they found a dual-hairpin eddy structure which appears as a combination of a "head-up" (H-U) and a "head-down" (H-D) hairpin vortex (Fig. 5). In between the counter-rotating legs of the corresponding hairpin, an ejection event ($u' < 0$, $v' > 0$) or a sweep event ($u' > 0$, $v' < 0$) are generated.

Despite the different physical properties, it seems that a comparable system of eddy structures manifests itself in aquatic canopies. Similar to the strategy of Finnigan *et al.* (2009) conditional averaging of the present fluid fields was performed. Here, the maximum deflection of the blades was used as the averaging condition. The result is shown in Fig. 7. In contrast to the observations of Finnigan *et al.* no dual-hairpin was observed, but only the H-D hairpin with a strong and pronounced sweep at the low-end between both counter-rotating legs. Nearly equivalent results were obtained for

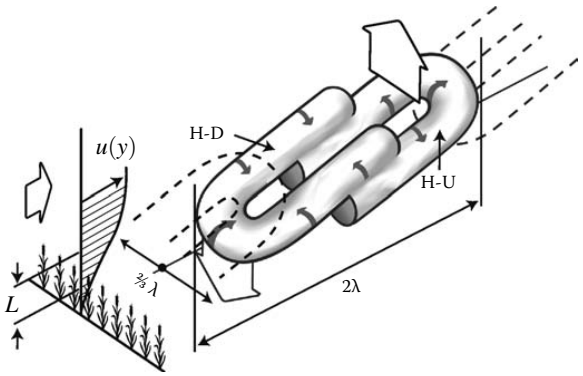

Figure 5. Dual-hairpin eddy model according to observations by Finnigan *et al.* (2009) for terrestrial canopies. The vortex structure consists of "head-up" (H-U) and "head-down" (H-D) hairpins aligned in streamwise direction. Due to the counter-rotating legs of the hairpins the H-U vortex generates an ejection, while the H-D hairpin generates a sweep. The broad arrows indicate the motion due to self-induction. The sketch was taken from the book of Fernando (2012).

different averaging conditions, especially sweep events and positive peaks of pressure fluctuations. Both events are strongly correlated with a maximal blade deflection and, hence, a *monami* event.
Besides the hairpin observed for the averaged fluid field, Fig. 7 shows instantaneous eddy structures for an arbitrary instant in time, visualized by iso-surfaces of negative pressure fluctuation $p' = \text{const}$. Obviously, hairpins cannot be found in the instantaneous flow fields. Rather, it appears that single "one-legged" eddies are formed in the shear layer located between a H-S streak and a L-S streak. The eddies are inclined in the downstream direction and turned over into a horizontal part at the top of the canopy. They resemble one half of the H-D hairpin. Indeed, since each H-S streak borders on two adjacent L-S streaks the eddy-formation is equiprobable on both sides, but not strictly arranged in pairs opposite each other. Currently, it seems that the two-legged hair-pin appears as a "statistical" artefact since the conditional average does not distinguish between differently directed "one-legged" eddies. Alternatively, it is also possible that both legs of the H-D hairpin are of different intensity, which is equalized by the averaging procedure. This could not be conclusively clarified and will be part of further work.

CONCLUSIONS AND FURTHER WORK

In the present study an immersed-boundary method for fluid-structure interactions of large numbers of flexible slender blades in turbulent flow was presented. The numerical method was applied to an aquatic submerged canopy flow corresponding to an experimental setup proposed by Okamoto & Nezu (2010*a*) which exhibits the *monami* phenomena. The three-dimensional flow data obtained were analyzed to develop a deeper understanding of the physics of flow-biota interaction in canopy flows. It was observed, that well separated large-scale high-speed streaks and low-speed streaks travel through the canopy prone to generate vortical structures. To extract statistically significant information conditional averaging was performed similar to the work of Finnigan *et al.* (2009). While in that reference terrestrial canopies were investigated, this is applied to aquatic canopies here. In contrast to observations by Finnigan *et al.* no dual-hairpin vortex was obtained, but only the lower part called "head-down" hairpin. In the instantaneous flow fields symmetric hairpins were not observed. Rather, it appears that instantaneous eddies are more shaped like one leg of a hairpin. This suggests that the symmetry of the hairpin is only the result of conditional averaging. To conclusively clarify this issue, further analyses of the data is under way, e.g. the use of an improved averaging condition and the evaluation of two-point correlations. The variation of physical parameters, e.g. the rigidity of the blades and the blade arrangement, will further elucidate the physical behavior. First studies reveal that high-speed streaks and low-speed streaks also occur in case of immobile rigid blades and more flexible blades. Moreover, configurations with spatially randomly distributed blades show a similar behavior, suggesting that the observed phenomena are somehow general properties of aquatic canopy flows.

REFERENCES

Antman, S.S., Marsden, J.E. & Sirovich, L. 2005 *Nonlinear Problems of Elasticity*. Springer.

Fernando, H.J. 2012 *Handbook of Environmental Fluid Dynamics, Volume One: Overview and Fundamentals*. CRC Press.

Finnigan, J.J, Shaw, R.H. & Patton, E.G. 2009 Turbulence structure above a vegetation canopy. *J. Fluid Mech.* **637**, 387–424.

Guendelman, E., Bridson, R. & Fedkiw, R. 2003 Nonconvex rigid bodies with stacking. *ACM Trans. Graph.* **22** (3), 871–878.

Kempe, T. & Fröhlich, J. 2012 An improved immersed boundary method with direct forcing for the simulation of particle laden flows. *J. Comput. Phys.* **231**, 3663–3684.

Lang, H., Linn, J. & Arnold, M. 2011 Multibody dynamics simulation of geometrically exact cosserat rods. *Berichte des Fraunhofer ITWM* **209**, 1–41.

Luhar, M. & Nepf, H.M. 2011 Flow-induced reconfiguration of buoyant and flexible aquatic vegetation. *Limnol. Oceanogr.* **56** (6), 2003–2017.

Okamoto, T. & Nezu, I. 2010*a* Flow resistance law in open-channel flows with rigid and flexible vegetation. In *Proceedings of the International Conference on Fluvial Hydraulics* (ed. A. Dittrich et al.), , vol. 1, pp. 261–268. Washington, D.C.: Bundesanstalt für Wasserbau.

Okamoto, T. & Nezu, I. 2010*b* Large eddy simulation of 3-d flow structure and mass transport in open-channel flows with submerged vegetations. *J. Hydro. Environ. Res.* **4**, 185–197.

Okubo, A. & Levin, S.A. 2001 *Diffusion and Ecological Problems: Modern Perspectives*. Springer.

Simo, J.C. 1985 A finite strain beam formulation. The three-dimensional dynamic problem. Part I. *Comput. Methods Appl. Mech. Engrg.* **49**, 55–70.

Tian, F.-B., Dai, H., Luo, H., Doyle, J.F. & Rousseau, B. 2014 Fluid–structure interaction involving large deformations: 3d simulations and applications to biological systems. *J. Comput. Phys.* **258**, 451–469.

Tonge, R., Benevolenski, F. & Voroshilov, A. 2012 Mass splitting for jitter-free parallel rigid body simulation. *ACM Trans. Graph.* **31** (4), 105:1–105:8.

Tschisgale, S. & Fröhlich, J. 2014 Simulation of a long slender structure in turbulent flow. *Proc. Appl. Math. Mech.* **14**, 499–500.

Turek, S. & Hron, J. 2006 Proposal for numerical benchmarking of fluid-structure interaction between an elastic object and laminar incompressible flow. In *Fluid-Structure Interaction. Lecture Notes in Computational Science and Engineering* (ed. HJ. Bungartz, M. Schäfer & (eds)). Springer.

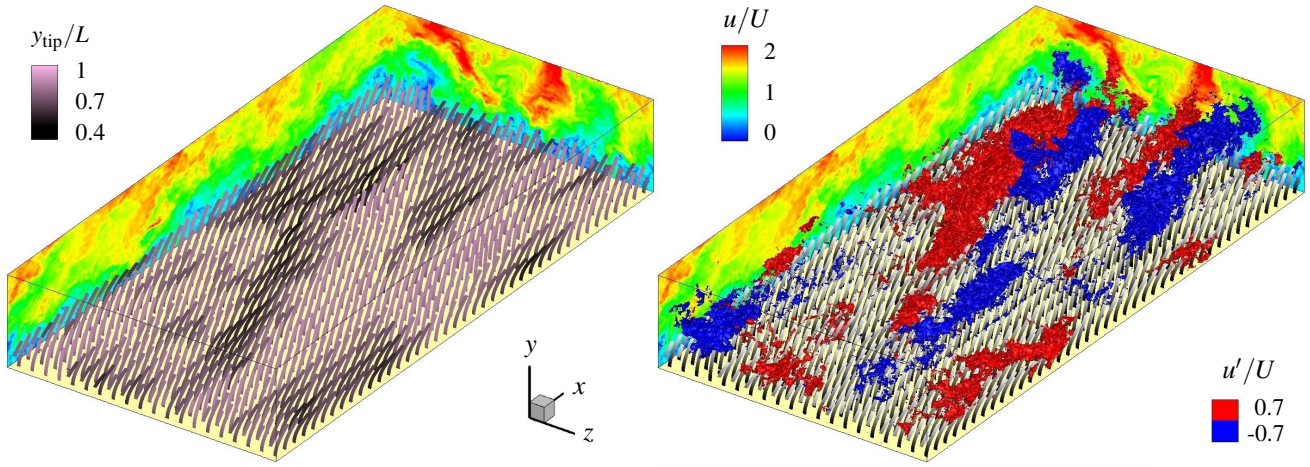

Figure 6. Large eddy simulation of a shallow submerged aquatic canopy in a turbulent channel flow, corresponding to the experimental setup of Okamoto & Nezu (2010*a*). Both visualizations show the instantaneous, streamwise velocity component u/U in the vertical planes $z = 0$ and $x = 6H$, at the same arbitrary instant in time t^*. In addition, the left figure shows the array of deflected blades colored with the respective normalized tip elevation y_{tip}/L. While some groups of blades are deflected by up to 50% of the blade length, other groups stand up quite vertically. In the right figure regions of positive and negative velocity fluctuation $u' = u - \langle u \rangle = \pm 0.7U$ are highlighted by iso-surfaces in red and blue, respectively.

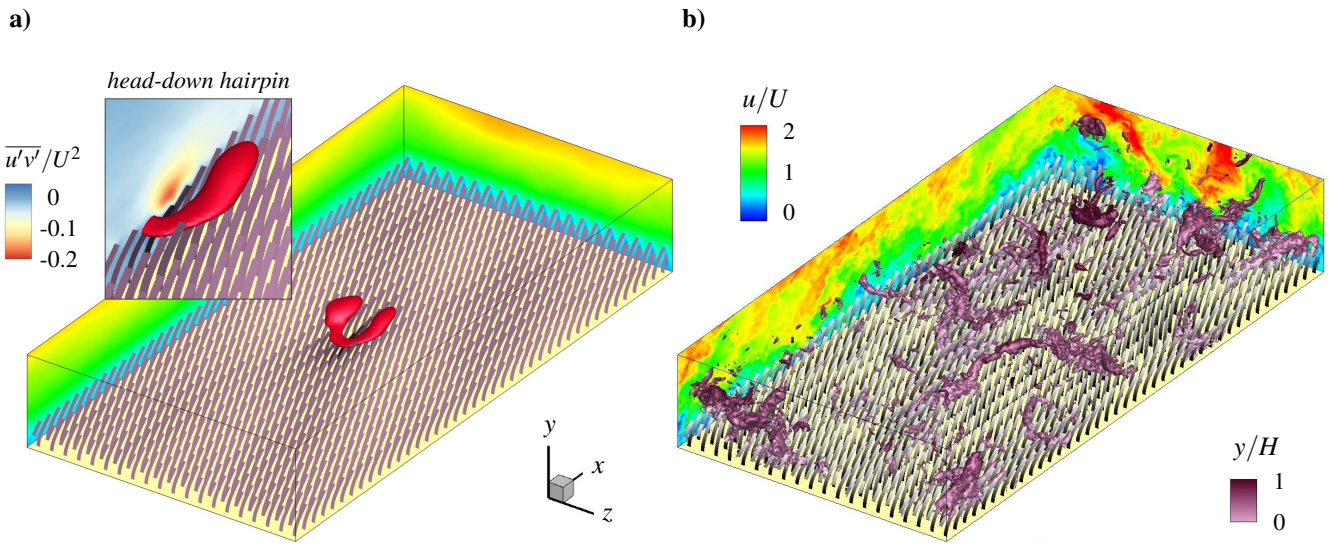

Figure 7. a) Conditionally averaged fluid field $\overline{u}/U$, where the events of high deflection are used as a trigger for an ensemble average. The flow fields have been transferred in horizontal direction such that the reference blade of highest deflection is located in the middle of the channel. The conditionally averaged surrounding blades are less deflected and blades further away exhibit the time averaged deflection shape. The region centered around the trigger blade reveals a H-D hairpin of width $3\Delta S$, visualized by an iso-surface of $\lambda_2 = -2.5$. Between the counter-rotating legs of the hairpin a sweep is generated, which yields a global minimum of the conditionally averaged Reynolds stress $\overline{u'v'}/U^2$ above the blade of highest deflection. In contrast to the work of Finnigan *et al.* (2009) no H-U hairpin occurs in combination with the H-D hairpin, as depicted in Fig. 5. b) Coherent vortex structures visualized by pressure iso-surfaces at a value $p'/\rho U = -0.2$ at the same instant in time t^* as in Fig. 6. A number of well separated eddies is observed ranging from the interior of the canopy far into the free flow region. The variation in height is colored with y/H. In the bottom region of the vortices the blades generally are highly deflected.